Eur. Phys. J. A **19**, 187–201 (2004)
DOI 10.1140/epja/i2003-10124-1

THE EUROPEAN PHYSICAL JOURNAL A

Broad states beyond the neutron drip line

Examples of ^{5}H and ^{4}n

L.V. Grigorenko[1,2,a], N.K. Timofeyuk[3], and M.V. Zhukov[4]

[1] GSI, Planckstrasse 1, D-64291, Darmstadt, Germany
[2] Russian Research Center "The Kurchatov Institute", 123182 Moscow, Russia
[3] Department of Physics, University of Surrey, Guildford GU2 7XH, UK
[4] Department of Physics, Chalmers University of Technology and Göteborg University, S-41296 Göteborg, Sweden

Received: 9 April 2003 / Revised version: 21 August 2003 /
Published online: 26 January 2004 –
Communicated by G. Orlandini

Abstract. Theoretical studies of broad states in the few-body systems beyond the neutron drip line have been performed. We introduce a theoretical model which allows to incorporate the initial structure of colliding nuclei, reaction mechanism, few-body effects and final-state interactions in studies of broad unbound states. The model is directly related to the sudden-removal approximation for high-energy knock-out or break-up reactions. We apply this model to qualitative studies of some general properties of broad few-body states including correlations for emitted fragments. The theoretical ideas are illustrated mainly using the example of ^{5}H. The prospect for observation of broad continuum structures corresponding to the tetraneutron ^{4}n is also discussed.

PACS. 21.45.+v Few-body systems – 21.60.Gx Cluster models – 25.10.+s Nuclear reactions involving few-nucleon systems

1 Introduction

With the recent progress in experimental techniques using radioactive beams, the frontiers of nuclear physics have been shifted to the edge of nuclear stability. For the review of the latest results obtained with radioactive nuclear beams see ref. [1]. For light nuclei, neutron and proton drip lines have been well established and the search for nuclear matter beyond the drip lines is continuing. Some progress has been achieved in this direction with the discovery of structures in the continuum beyond the neutron drip line corresponding to the formation of ^{10}He [2], ^{5}H [3–5], ^{7}H [6]. It is clear that further experimental discoveries of similar few-body systems will be made in the future.

Matter beyond the neutron drip line manifests itself as broad structures in the few-body continuum. The widths of such structures can in some cases be as large as several MeV. Therefore, the properties of broad few-body structures or resonances should be reviewed and understood from the point of view of the latest achievements in nuclear few-body physics.

One important definition of a state (let us call it "an ordinary state") is that the state properties do not depend on the observation conditions (or on how the state has been produced). For sufficiently narrow states such independence can be proved under the assumption that wave functions are concentrated in regions where the interactions are strong. For broad states, such independence is no longer guaranteed because of the specific origin that these states could have. For example, the formation of broad states could be caused by slow motion in the internal region and tunneling between multiple channels rather than reflection from some potential barrier. So, one should speak about "structures in the continuum" or "continuum response", rather than states (in this paper, however, we are not very strict about this terminological difference).

Available theoretical methods of treating the resonances in the continuum deal with quantities like energies in the box, S-matrix for $A \to A$ scattering, poles of S-matrix and the zeros of Jost functions. In the case of broad states, these quantities cannot be easily related to experimental observables and all the three ingredients of reaction theory become important: i) initial structure, ii) reaction mechanism, and iii) final-state interaction (FSI).

In this paper we discuss the problems which arise in the interpretation of broad states in the traditional few-body approach (sect. 2), and then make an attempt to combine all the three aspects, mentioned above, in a simplified and qualitative but methodologically consistent model. We introduce into the Schrödinger equation, traditionally used to describe the properties of few-body systems, a source

[a] e-mail: L.Grigorenko@gsi.de

term which takes into account a reaction mechanism, that produces the few-body system, and explicitly depends on the internal structure of the parent nuclei. We apply our theoretical model to describe broad structures in the ^{5}H (sect. 3) and ^{4}n (sect. 4) continuum assuming that they have been formed in high-energy knock-out (break-up) reactions. In this paper we concentrate mainly on the theoretical issues of our model. The forthcoming paper [7] is dedicated to a discussion of the current experimental situation with studies of the ^{5}H system, which is rather complicated [3–5].

Since no bound subsystems exist in ^{5}H (treated as $^3\mathrm{H}+n+n$) and ^{4}n, the Hyperspherical Harmonic method (HH) is used to solve equations of the model. The details of the HH method, its notations relevant to the material of the paper and necessary references are given in appendix A. The details of the models for ^{5}H and ^{4}n can be found in [8] and [9], respectively. In appendices B-D we study the formal questions of the model we use in different physical assumptions. The system of units $\hbar = c = 1$ is used in the article.

2 Continuum structures in ^{5}H from the conventional point of view

Previous theoretical studies of ^{5}H concluded that it is particle-unstable [10–13,8,14] and has $1/2^+$, $5/2^+$ and $3/2^+$ spin ordering (see table 1). The predictions of peak positions and widths from cluster model calculations [8, 14] are in reasonable agreement with each other.

Since ^{5}H is unbound with respect to the $t+n+n$ decay, it should be studied with the help of the 3-body Shrödinger equation

$$\left(\hat{H}_3 - E_{\mathrm{T}}\right)\Psi_3 = 0\,, \tag{1}$$

where $\hat{H}_3$ is a three-body Hamiltonian and E_{T} is the total 3-body energy. The best way to solve this equation for ^{5}H is to use the hyperspherical harmonics method. This method leads to the coupled set of differential equations

$$\left[\frac{\mathrm{d}^2}{\mathrm{d}\rho^2} - \frac{\mathcal{L}(\mathcal{L}+1)}{\rho^2} + 2M\left\{E_{\mathrm{T}} - V_{K\gamma,K\gamma}(\rho)\right\}\right]\chi_{K\gamma}(\rho) = \sum_{K'\gamma'} 2MV_{K\gamma,K'\gamma'}(\rho)\chi_{K'\gamma'}(\rho)\,, \tag{2}$$

where ρ is the hyperradius, $\mathcal{L} = K + 3/2$ and $V_{K\gamma,K'\gamma'}(\rho)$ are the matrix elements of the sum of the pairwise potentials (we refer to them as to three-body potentials) fitted to the t-n and n-n scattering data [15,16]. More details on this method, references and notations associated with it can be found in appendix A.

2.1 ^{5}H as a ground state in a box

First of all, we would like to show to what extent proper consideration of asymptotic conditions is important for broad resonances. To do this, we solve eq. (2) with zero boundary condition at large values of ρ. The solid line in fig. 1 shows the ground-state energy of ^{5}H, calculated in such a box, as a function of the box size ρ_{box}. The ground-state energy monotonously decreases when the box size increases which means that no states exist in such a calculation.

Table 1. States in ^{5}H relative to the $t+n+n$ threshold (energies and widths of the states are given in MeV).

Method	$1/2^+$		$3/2^+$		$5/2^+$	
	E	Γ	E	Γ	E	Γ
Shell model [10]	5.5					
Shell model [11]			10.5		7.4	
HH, 5-body [12]					6	~ 6
RGM [13]	~ 6	> 4				
HH, $3 \to 3$ [8]	~ 2.7	~ 3	~ 6.6	~ 8	~ 4.8	~ 5
GCM [14]	~ 3	1–4				
HH, 5-body [9]	~ 2					

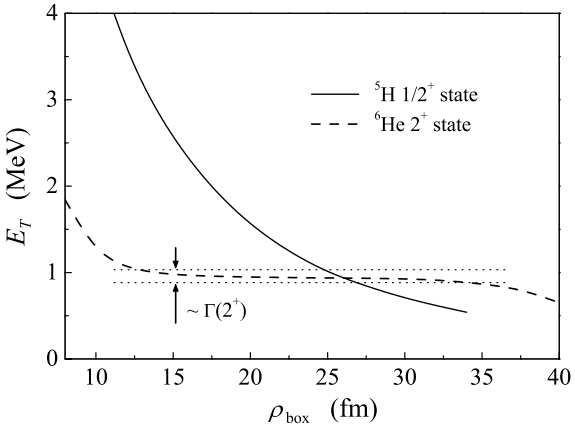

Fig. 1. Energy of the ^{5}H ground state calculated in a box *versus* the box size ρ_{box} (solid curve). The same for the well-defined 2^+ state in ^{6}He is shown by the dashed curve.

For comparison, we have calculated energies of the 2^+ state in ^{6}He in a box, using exactly the same input as in [17], and plotted them in fig. 1 as well. The energy ^{6}He 2^+ stabilizes with increasing ρ_{box}, thus showing formation of a narrow quasistationary state. The width of this state (about 100 keV) can be determined from this curve with a good precision as an uncertainty of the state position. When ρ_{box} comes out of a barrier, the ^{6}He 2^+ energy tends to zero and the radius of ^{6}He infinitely increases.

This example shows that the energy of the ^{5}H ground state cannot be determined in a model which does not take boundary conditions into account. The same problem may occur if other models, for example, five-body models without three-body asymptotic conditions, are used for the ^{5}H study. The fact that ^{5}H is not particle-stable is already included in the five-body Hamiltonian and without proper asymptotic three-cluster conditions the accuracy of the position of the ^{5}H "ground state" cannot be determined to a precision better than the ^{5}H width. Besides, another danger of such calculations is that the ground-state energy

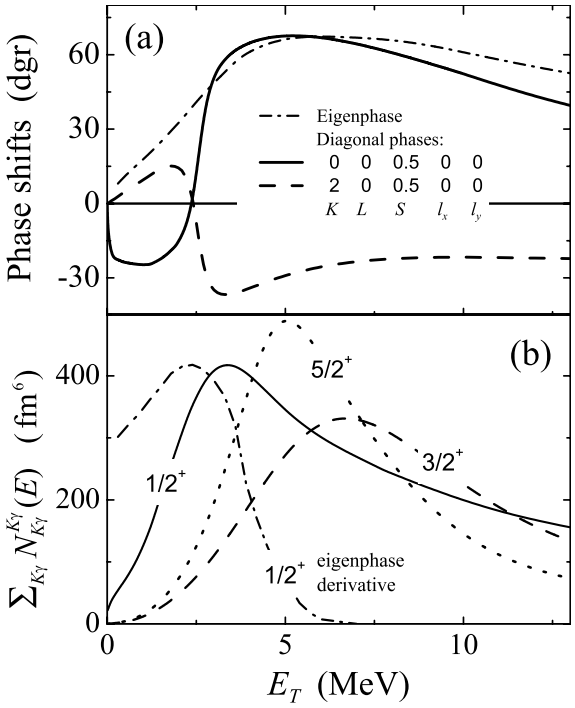

Fig. 2. Panel (a): the diagonal phase shifts $\delta^{K\gamma}_{K\gamma}$ for the $1/2^+$ state of ^{5}H and the lowest eigenphase. Panel (b): the internal normalizations for $1/2^+$, $5/2^+$, and $3/2^+$ states obtained in the $3 \to 3$ calculations, ref. [8]. The energy derivative of the eigenphase for the $1/2^+$ state (see panel (a)) is in arbitrary units.

of ^{5}H may fall on the $t+n+n$ threshold if the model space used infinitely increases.

2.2 Conventional way: 3 → 3 scattering

We have studied the $3 \to 3$ scattering for the ^{5}H system within the HH method in our previous work [8]. Some results from this work are shown in fig. 2. It can be seen in this figure that some diagonal phase shifts in the channels with the lowest quantum numbers change very rapidly. Structures in the continuum associated with such a behaviour of the phases for an isolated channel should have widths of about 600 keV. However, such behaviour of the selected phases does not guarantee the appearance of the three-body resonance: the behaviour of the lowest eigenphase is smooth and its maximal value barely exceeds 60 degrees. The eigenphase energy derivative is sometimes used to characterize the resonances in the systems with coupled channels. It gives a broad structure with maximum at about 2.3 MeV (fig. 2b). If we look at the other continuum fingerprint —internal normalizations of the scattering WFs— we can also see broad responses. However, the maximum energy for internal normalization for $1/2^+$ state is about 3.3 MeV. The internal normalizations is a simplified measure of the overlap integrals in the transition amplitudes for various processes with three particles in the final state [18]. They describe the energy behaviour of the transition matrix elements for the reactions qualitatively well; they can be considered as a more realistic characteristic of the resonance. It was concluded in [8], that the experimentally observable signature for ^{5}H should be quite broad.

What we want to emphasize here is that the different types of values characterizing the continuum for $3 \to 3$ scattering give drastically different properties for the ^{5}H ground state. Below we move along this line considering ^{5}H also in a different model.

3 ^{5}H in the model with source (MWS)

3.1 Motivation

The conventional way of studying the properties of ^{5}H via $3 \to 3$ scattering would be perfectly acceptable if such reactions were experimentally achievable. In reality, continuum structures corresponding to ^{5}H have been observed either in ^{6}He break-up [3,5] or in two-neutron transfer reactions [4]. The ^{5}H formed there does not live long enough to "forget" the way it was populated. To illustrate this, let us make the following simple estimations.

The "time of flight" for a particle with kinetic energy $T_{\rm kin}$ moving in a potential well is

$$t = r_{\rm int}\sqrt{M/(2T_{\rm kin})} \approx 0.11\, r_{\rm int}\, T_{\rm kin}^{-1/2}\,, \qquad (3)$$

where $r_{\rm int}$ is the distance between the classical turning points. To form a state with a well-defined internal structure, the particle should reflect many times from the barrier. Let it be, for example, ten reflections. For a standard two-body nuclear problem $T_{\rm kin}$ is 40–60 MeV and $r_{\rm int}$ is about 3–6 fm. This means that for widths larger than 1–2 MeV the number of reflections is less than ten. For few-body resonances the flight distance is of order of the hyperradius $\rho_{\rm int}$, where $\rho_{\rm int}$ is the distance between the classical turning points in a hyperspherical potential well

$$V_{K\gamma,K\gamma}(\rho) + \mathcal{L}(\mathcal{L}+1)/\rho^2\,,$$

see eq. (2). The hyperradius $\rho_{\rm int}$ should be larger than the two-body radius $r_{\rm int}$ and can be estimated as 5–10 fm. On the other hand, the average depth of the three-body potential well U_0 is much smaller and the kinetic energy $T_{\rm kin} = E_{\rm T} - U_0$, where $E_{\rm T}$ is the resonance energy above the threshold, is only about 3–6 MeV. These estimates have been taken from the calculations of the 2^+ state in ^{6}He or the ground state of ^{6}Be [17]. Therefore, in the case of weakly bound three-body systems, the number of reflections is less than ten for widths larger than 200–500 keV.

These estimates outline a not often appreciated fact that there is a qualitative difference between two-body and few-body resonances. The underlying dynamics implies that narrow few-body resonances correspond in reality to much broader two-body states. Typical (quite narrow) three-body resonances like the 2^+ state in ^{6}He or the 0^+ ground state in ^{6}Be with widths of about 100 keV actually have dynamics which are typical of much

broader (500–800 keV) two-body resonances. In particular, for structures broader that 1 MeV, which is definitely the case of ^{5}H, the number of reflections is only 2 to 5. Therefore, the decay spectrum for such systems can be influenced by the mechanism of the reaction in which this system is formed. Below we suggest a possible way to deal with this problem.

3.2 MWS

In the present paper, we assume that ^{5}H is created from ^{6}He by the sudden removal of a proton from the α-core in a high-energy knockout or break-up reaction. In such a process the wave function of ^{5}H at $t_0 = 0$ should be the same as that of ^{6}He, but then it should evolve according to the three-body Hamiltonian $\hat{H}_3$ of ^{5}H. However, instead of solving the time-dependent problem, we introduce a compact source function $F_{^5\mathrm{H}}^{J^\pi}$ on the right-hand side of the stationary Schrödinger equation (1) and solve the inhomogeneous equation

$$\left(\hat{H}_3 - E_\mathrm{T}\right)\Psi_3^{(+)} = F_{^5\mathrm{H}}^{J^\pi} \tag{4}$$

for pure outgoing-wave boundary conditions. Intuitive motivations for such reformulation of the problem is that i) only outgoing few-body waves are realized in experiments and ii) reaction volume which forms the outgoing waves of few particles has a limited size. All the formal issues associated with this reformulation are considered in appendix B.

For reactions, in which ^{5}H is produced from ^{6}He, the source term $F_{^5\mathrm{H}}^{J^\pi}$ should contain the Fourier transform of the overlap integral between the triton wave function Ψ_t, spin-isospin function of proton χ_p and the ^{6}He wave function over the radius-vector $\mathbf{r}$ between the removed proton and the center of mass of ^{5}H:

$$F_{^5\mathrm{H}}^{J^\pi} \sim \Phi_{^5\mathrm{H}}^{1/2^+} = \int \mathrm{d}\mathbf{r}\, e^{i\mathbf{qr}} \langle \Psi_t \chi_p | \Psi_{^6\mathrm{He}} \rangle\,. \tag{5}$$

In general, this quantity should be a complicated function of the vector of the recoil momentum, transferred to the ^{5}H system in the proton removal process. However, at present, we assume that the ^{5}H recoil momentum is negligible and the source term does not contain any other kinematic factors. We understand that such an approach oversimplifies the problem but, on the other hand, we do not see any immediate necessity for a more complicated source term since we are interested only in qualitatative features of the problem.

The excitation spectrum of ^{5}H formed in the break-up channel should be proportional to the outgoing current of three particles on a hypersphere $\rho = a$:

$$j(a) = \frac{1}{M}\,\mathrm{Im} \int \mathrm{d}\Omega_\rho \mathrm{d}\Omega_\kappa\, \Psi_3^{(+)\dagger} \rho^{5/2} \frac{\mathrm{d}}{\mathrm{d}\rho}\, \rho^{5/2}\, \Psi_3^{(+)} \Big|_{\rho=a}\,. \tag{6}$$

For a sufficiently large hypershere radius, this current should not depend on a and can be expressed via the asymptotic amplitudes $A_\gamma^K(E_\mathrm{T})$ (see appendix A for their definition):

$$j(a) = \sqrt{2E_\mathrm{T}/M}\ \textstyle\sum_{K\gamma} |A_\gamma^K(E_\mathrm{T})|^2\,. \tag{7}$$

This expression is formally equivalent to the following one:

$$j(a) = \frac{1}{\sqrt{2M^3 E_\mathrm{T}}} \textstyle\sum_{K\gamma} \left| \sum_{K'\gamma'} \int \mathrm{d}\rho\, \chi_{K\gamma}^{K'\gamma'}(\kappa\rho) f_{K'\gamma'}(\rho) \right|^2,$$

in which $\chi_{K\gamma}^{K'\gamma'}(\kappa\rho)$ are the solutions of the homogenous Schrödinger equation.

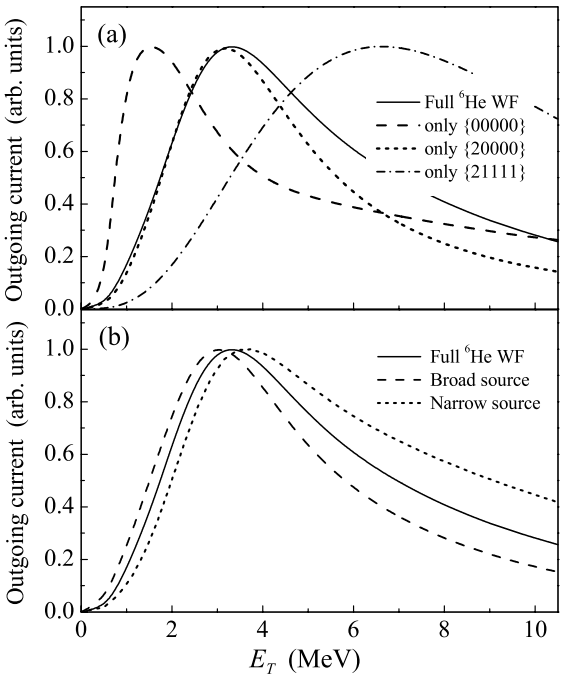

Fig. 3. Outgoing current of ^{5}H $J^\pi = 1/2^+$ given by eq. (7) of the MWS for proton removal from ^{6}He. Calculations demonstrate sensitivity to the source function choice: (a) different HHs $\{K\ L\ S\ l_x\ l_y\}$ and (b) different source sizes (normal size and $\pm 10\%$.

3.3 Outgoing current and correlation spectra

We have calculated the outgoing current of the MWS using the same Hamiltonian $\hat{H}_3$, as in the $3 \to 3$ scattering problem [8], and the source term represented by the three-body wave functions of ^{6}He from ref. [17]. We expect that the center-of-mass recoil does not influence the source term very much. This is qualitatively confirmed by modelling this recoil in the simple model of appendix C.

The calculated outgoing current is shown in fig. 3 by the solid line. It resembles the missing-mass spectrum obtained in [8] in a simplified model for the vertex of the ^{5}H production. To estimate how the neglected center-of-mass recoil changes the results of our calculations, we have

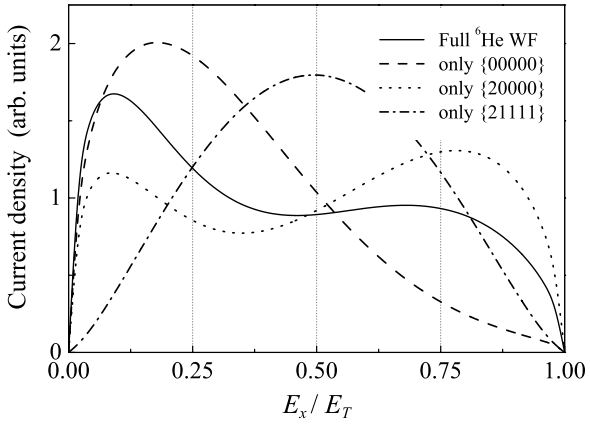

Fig. 4. Correlation spectra for different kind of sources. E_x is the energy between two neutrons and the energy of the triton is $2/5(E_{\rm T} - E_x)$. The solid curve shows the results for the full source function. The dashed, dotted, and dash-dotted curves correspond to a single HH with $\{K\ L\ S\ l_x\ l_y\}$ as a source. Each spectrum is calculated for the energy $E_{\rm T}$ taken at the peak energy for the corresponding curve in fig. 3a.

modified the size of the source by making it broader or narrower by 10%. The sensitivity to the source size, demonstrated in fig. 3b, is moderate and corresponds to the sensitivity found in [8].

Now we investigate how different components of the ^{6}He wave function influence the shape of the outgoing current and, therefore, the excitation spectra. As far as different components of ^{6}He have quite different correlations, these correlations can be seen under different experimental conditions. To do this, we use only some components of the ^{6}He wave function as a source (fig. 3a). The case, where only the $\{K=0, L=0, S=0, l_x=0, l_y=0\}$ component is used (dashed curve in fig. 3a), corresponds to emission from an uncorrelated source with a size of ^{6}He. The uncorrelated source is a standard assumption, for example, in particle intensity interferometry [19]. Our calculations show that the corresponding continuum structure would be the narrowest, having a low energy peak about 1.5 MeV. If we only take the $\{K=2, L=0, S=0, l_x=0, l_y=0\}$ component (dotted curve), this corresponds to the pure $0\hbar\omega$ structure of ^{6}He. This component gives the main contribution to the shape of the outgoing current. The dot-dashed curve corresponds to the situation when ^{5}H is produced only from the $S=1$ component of the ^{6}He wave function in the knock-out reaction. The corresponding excitation spectra would have a very broad continuum response in this case.

Different components of ^{6}He are also responsible for different specific shapes of the correlation spectra. We have shown in fig. 4 the correlation spectra which correspond to the source functions constructed from different hyperharmonics. The correlation spectra are calculated at the peak energies for each of the sources (as shown in fig. 3). To achieve a stability of the relative energy distributions, the calculations have been carried out up to

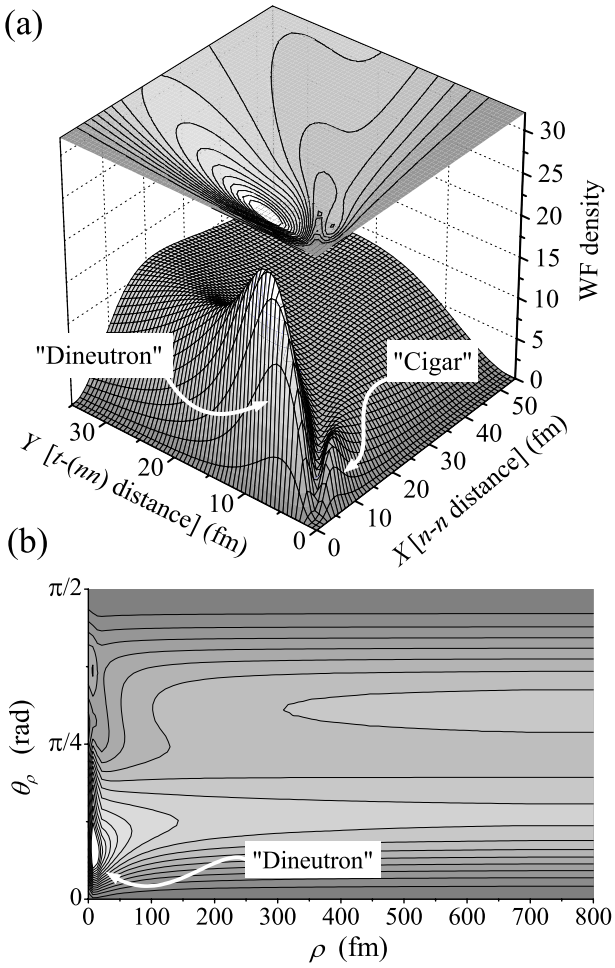

Fig. 5. The spatial densities for $1/2^+$ state in ^{5}H at $E_{\rm T} = 3$ MeV obtained in the MWS with full wave function of ^{6}He. (a) shows the density multiplied by ρ on the XY plane. Such density should tend to a constant (rather than as $1/\rho$) at large ρ on the XY plane. (b) shows the convergence of the density at large hyperradii as a function of the hyperangle θ_ρ. Small values of the hyperangle mean that neutrons are close to each other.

hyperradius $\rho \sim 600$ fm and hypermoment $K_{\rm max} \sim 26$–30. The shapes of the correlation spectra produced due to the knock-out from different components of ^{6}He differ enough to be distinguished experimentally.

3.4 ^{5}H as a remnant from ^{6}He

If we neglect for a moment the spin of the ^{3}H core, ^{5}H could be considered as $^3\mathrm{H}+2n$ in analogy with the neighbouring neutron halo ^{6}He nucleus ($^4\mathrm{He}+2n$), since in both cases we have the s-wave Pauli repulsion in the $^3\mathrm{H}+n$ and $^4\mathrm{He}+n$ subsystems and attraction in p-waves. The $^3\mathrm{H}+n$ interaction for the p-wave is weaker than that for $^4\mathrm{He}+n$ so we can expect the states analogous to the 0^+ ground state and 2^+ 1.8 MeV state in ^{6}He to be lifted up in ^{5}H to the continuum. Thus taking into account the spin of ^{3}H we can expect $1/2^+$ as a "ground state" and

instead of 2^+ in ^{6}He we can expect the doublet $3/2^+$ and $5/2^+$, based on the same orbital configuration.

If ^{5}H and ^{6}He have a similar structure, one can expect that the most effective population of the ^{5}H continuum should happen when ^{5}H is produced from ^{6}He, for example, in proton knock-out reactions. We have calculated the spatial densities of the ^{5}H ground state in the MWS with the full ^{6}He wave function used as a source. These densities are concentrated in the internal region whose size $\rho_{\rm int}$ can be considered to be about 15–20 fm (see fig. 5). For "real" (narrow) resonances such concentration is, of course, much stronger and densities are concentrated at smaller $\rho_{\rm int}$. The shapes of the coordinate correlations somehow resemble those in ^{6}He (see [17], for example). There are "dineutron" (the neutrons are close to each other) and small "cigar" (neutrons are sitting on the opposite sides of the core) correlations. The "dineutron" peak is more pronounced in the ^{5}H density, than in ^{6}He, which means that the n-n interaction is more important in the ^{5}H dynamics. It is useful to note here that internal structures in ^{5}H are developed despite the fact that its lifetime corresponds only to a few reflections within a shallow potential well.

3.5 Width and lifetime

The MWS predicts quite a broad structure for the ^{5}H ground state in the excitation spectra. The width of this structure is between 2 and 4 MeV, depending on the width of the source term. Alternatively, the width can be determined as the inverse lifetime of a system. For quasistationary states the time dependence of the wave function can be described as

$$\Psi^{(+)}(r_i,t) = \exp[iEt - \Gamma t/2]\,\Psi^{(+)}(r_i) \qquad (8)$$

and the width Γ can be obtained by applying Green's theorem to the Schrödinger equation (4). According to [20,21], for three-body systems this procedure gives

$$\Gamma = \frac{j(\rho_{\rm int})}{N(\rho_{\rm int})} \quad N(\rho_{\rm int}) = \int {\rm d}\Omega_\rho {\rm d}\Omega_\kappa \int_0^{\rho_{\rm int}} {\rm d}\rho\, \rho^5 |\Psi_3^{(+)}|^2, \qquad (9)$$

where the function $\Psi_3^{(+)}$ should be taken at the resonance energy. Equation (9) has a simple physical meaning: for systems obeying the exponential decay law, the width is the ratio of the current through a hypersphere of a large radius to the number of particles inside it.

We have calculated the ^{5}H width in the MWS using the definition (9) and plotted it in fig. 6 as a funciton of $\rho_{\rm int}$. At large values of $\rho_{\rm int}$ the width (9) behaves as $1/(\text{const} + \rho_{\rm int})$ because the contribution of $\Psi_3^{(+)}$ to the normalization grows linearly with the integration limit. This dependence is unphysical because the width should not depend on $\rho_{\rm int}$ if the latter is large enough. Therefore, $\rho_{\rm int}$ should be limited by some typical size of a "nuclear interior" which ranges from 15 to 20 fm for the case of ^{5}H. Figure 6 shows that after 15 fm the widths corresponding to the sources of different size are close to each other and the behaviour of the width curves stabilizes. The stability

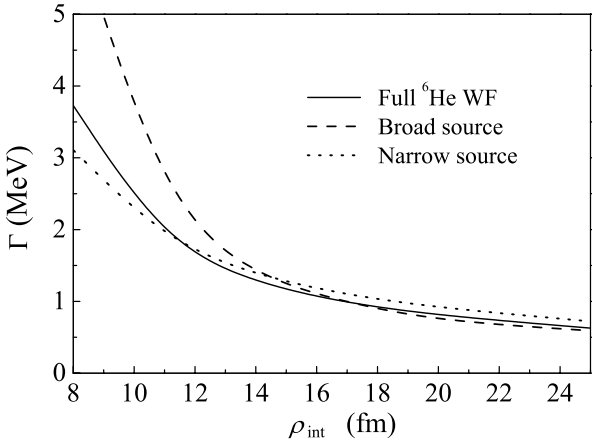

Fig. 6. Width defined via lifetime by eq. (9) as a function of the parameter $\rho_{\rm int}$. Curves of different styles correspond to those from fig. 3b.

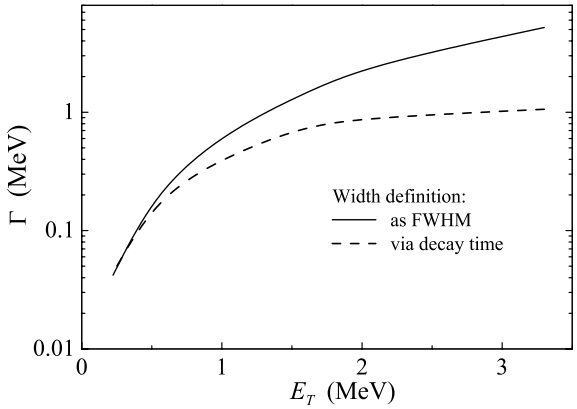

Fig. 7. The width of ^{5}H defined via decay time (dashed line) and as the FWHM of the MWS calculations (solid curve) as a function of the peak energy of the resonance. The two widths converge at small energies.

of the results obtained means that the definition (9) is usable even though our case is beyond the assumptions in which this definition has been obtained. The widths provided by the definition (9) are between 0.7 and 1.3 MeV which is lower than the widths of the excitation functions from fig. 3b calculated in the same model.

The difference between the different definitions of the width as a function of the peak energy of the resonance is illustrated in fig. 7. In these calculations the binding of ^{5}H was artificially increased by including an attractive three-body potential,

$$V_{K\gamma,K'\gamma'}(\rho) = \delta_{K\gamma,K'\gamma'} V_3^0/[1+(\rho/\rho_0)^3]\,, \qquad (10)$$

into $\hat{H}_3$. At $E_{\rm T} < 0.5$ MeV, the two definitions predict the same width. Let us note that $E_{\rm T} \sim 0.5$ MeV corresponds well to the simple estimates made on the basis of a time of flight of a slow particle in a shallow three-body potential well given by eq. (3). So, we can expect that the resonance in ^{5}H can become "normal" only below

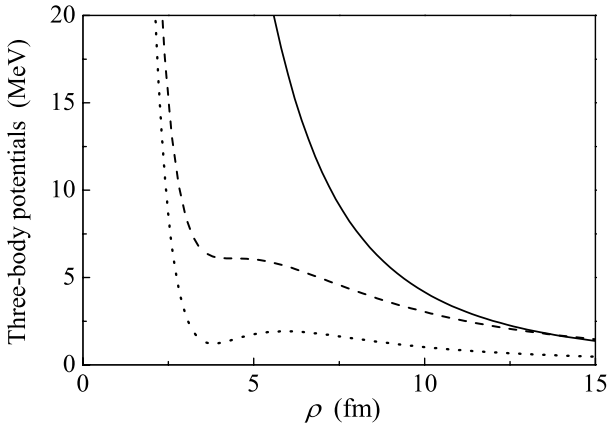

Fig. 8. Three-body diagonal potentials $V_{K\gamma,K\gamma}(\rho)$ for $K = 0$ (solid curve) and $K = 2$ (dashed curve). The diagonalized potential is given by the dotted curve.

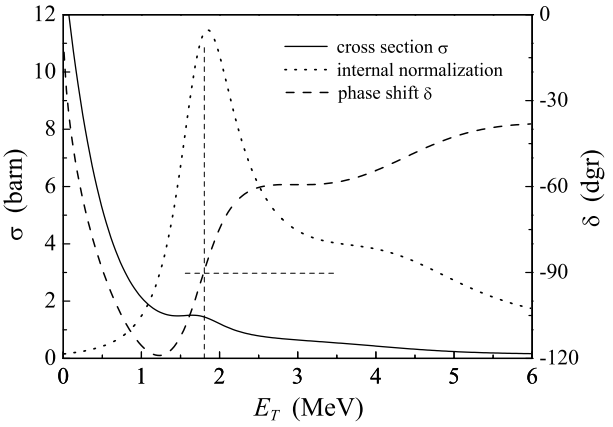

Fig. 9. Continuum properties for two-body s-wave scattering for repulsive square potential $V_0 = 1$ MeV, $r_0 = 15$ fm. The radius for the internal normalization is 7 fm.

$E_{\rm T} = 0.4$–0.6 MeV. However, theoretical calculations lead to a much larger energy, $E_{\rm T}$, which is of the order of 3 MeV. For this energy, the width of ^{5}H as a FWHM of the MWS calculations is about four times larger than the width obtained via the lifetime.

3.6 Discussion

3.6.1 ^{5}H as a "multichannel" resonance

Usually, resonances are formed because a time is needed for a system to tunnel through some potential barrier. About 30 years ago the possible existence of another type of resonances was suggested in ref. [22]. These resonances arise in a multichannel problem where transitions between numerous channels can generate a significant time delay in the decay of a system. It was shown in ref. [22] that such multichannel resonances (or resonances of the second kind) are characterized by some long-range "interaction" which makes their properties significantly different from those of "normal", or short-ranged, resonances.

^{5}H is a good example of a resonance of the second kind. Its diagonal three-body hyperradial potentials $V_{K\gamma,K'\gamma'}(\rho)$ are repulsive in all channels. In the $K = 2$, $L = 0$, $l_x = l_y = 0$ channel, this repulsion is minimal, but this channel on its own allows formation of continuum structures only at energies larger than 7 MeV. Only interactions with other channels provide sufficient enhancement in the low-energy spectrum, which is qualitatively illustrated by the diagonalized potential in fig. 8. It has a shallow broad pocket with the bottom at 1.2 MeV, making the excitation spectrum with peak at about 3 MeV possible. From this point of view, ^{5}H is similar to the 1^- continuum of ^{6}He, for which a more detailed discussion of this phenomenon can be found in [18].

3.6.2 ^{5}H waves in "shallow water"

The broad and shallow diagonalized potential, which makes the formation of the multichannel resonance ^{5}H possible, has such a tiny barrier that the fact that ^{5}H does not immediately decay looks at first sight surprising. Let us note, however, that sharp resonance-like structures in the continuum can be formed *even without any barriers*. Moreover, they can be formed if *only repulsive* potentials are present in the system.

This point is well illustrated in the classical textbook of Flügge [23]. Let us consider the two-body s-wave scattering on a repulsive square barrier potential $V(r) = V_0$ for $r < r_0$ and $V(r) = 0$ for $r > r_0$, which is very weak ($V_0 \sim 1$ MeV), but very broad ($r_0 \sim 15$ fm). The phase shift for such a scattering passes -90 degrees at about 1.7 MeV (see fig. 9), but this produces only a minor enhancement in the scattering cross-section because the "shadowing" effect of the broad repulsive potential at low energies is enormous compared to the resonance-like structure. However, the resonance-like narrow peak is clearly seen in the internal normalization of the wave function and since it is the internal normalizations that generate energy dependence of matrix elements of different processes, this peak must be perfectly observable if populated in some reactions.

From a formal point of view, the resonance-like structure (or the anomaly in the continuum) is connected with interference effect. The waves, reflected from the origin and from the front surface of the flat part of the repulsive potential ("potential shelf"), strongly iterfere when an integer number of half-waves is present inside the potential shelf. Qualitatively, the abnormal continuum behaviour can be associated with the slow motion of a particle above the potential shelf which creates the concentration of the wave function in the internal region. Such a phenomenon drastically differs from the case of ordinary resonances. For them, internal motion is much more rapid than the external one and the wave function is concentrated in the internal region due to multiple reflections from the barrier. In some sense, the concentration of the wave function above the shelf looks like waves rising high in shallow water.

The two-body case, considered above, has a relevance to the ^{5}H problem. In a single-channel approximation, the

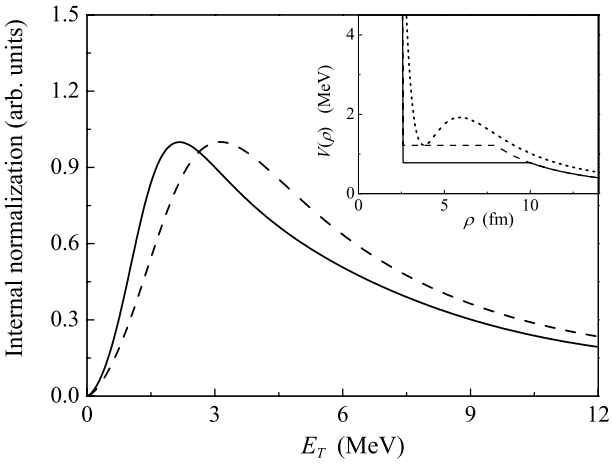

Fig. 10. Continuum properties for potentials (shown in the inset), imitating the diagonalized hyperspherical potential of fig. 8. The maximal hyperradius for the internal normalization is 15 fm. The potentials corresponding to the curves of the same style are shown in the inset. The dotted curve shows the diagonalized potential from fig. 8 for comparison.

effective hyperradial potential for ^{5}H looks very similar to the broad repulsive shelf, although it has a small attractive pocket (see fig. 8). The internal normalization obtained in the single-channel calculations with a potential, which behaves as hyperspherical centrifugal barrier with $K = 0$ but has a broad constant shelf (see inset in fig. 10), is very similar to those obtained in exact three-body calculations (see fig. 2b). However, in order to get a peak at 3.5 MeV in the "shallow water" approximation, a stronger attraction is required and the potential shelf should be deeper than the real diagonalized three-body potential. This means that the "shallow water" effect does not entirely govern the behaviour of the ^{5}H continuum, the multichannel aspects also being important.

4 Perspectives of observation of the tetraneutron

4.1 Current situation

The search for the tetraneutron ^{4}n has been unsuccessful for the last 40 years. Very low upper limits on the cross-section of the bound tetraneutron production have been obtained for the pion double charge exchange $^4\mathrm{He}(\pi^-,\pi^+)$ [24,25] and in a number of transfer reactions [26,27]. The missing-mass spectra of the ^{4}n particle have also been studied in order to find a deviation from the phase volume behaviour. In some experiments a deviation was found [24], while in others the missing-mass spectrum had exactly the phase volume character [26]. A very strong argument against the existence of the bound ^{4}n is the fact that ^{5}H is unbound. However, recent possible detection of multineutron clusters in the fragmentation of ^{14}Be on the carbon target [28] has attracted attention to the tetraneutron problem again.

Theoretically the nonexistence of the bound ^{4}n has been confirmed many times [29–33]. The most recent work [33], in which the ^{4}n problem has been studied in the Green's Functions Monte Carlo method with the best available NN and NNN interactions, states that modern nuclear Hamiltonians cannot tolerate a bound tetraneutron, but hints that a very broad-resonance ^{4}n state may exist at 2 MeV. This state has been obtained by the extrapolation of the ^{4}n energy calculated in an external potential well.

Searches for resonances in the ^{4}n continuum, based on the theoretical treatment of the $4 \to 4$ scattering, have also been performed [34–38]. Almost all of them used the $K = K_{\min}$ approximation of the HH method but only in ref. [37] the calculations were made in the $K = K_{\min} + 4$ basis. No resonances were found when the NN potential used did not bind the dineutron, except in ref. [38], where complex energies with negative real, but large imaginary parts were obtained. Proper ^{4}n resonances were found only for the NN potential that binds the dineutron [37]. The only attempt to take a reaction mechanism into consideration of the ^{4}n structure has been done in [34,35], where the importance of the four-neutron FSI for the cross-section at different kinematic conditions was demonstrated. Since broad-resonance structures in the continuum are of multichannel character, a large model space is required in searches for ^{4}n. Therefore, all the conclusions made in previous works within the $K = K_{\min}$ approximation should be considered as very preliminary.

4.2 Tetraneutron in MWS

To understand if any effect of the final-state interaction of four neutrons in the continuum could be observable, we study the emission of four neutrons by some source in a knock-out or break-up reaction. We assume that ^{4}n is created after the sudden removal of an α-particle from ^{8}He. Simple model wave functions for this nucleus are available in the COSMA model [39]. The MWS for such a process is

$$\left(\hat{H}_4 - E_T\right) \Psi_4^{(+)} = F_{^4\mathrm{n}}^{0^+} \,, \tag{11}$$

in which the wave function $\Psi_4^{(+)}$ is expanded in the hyperspherical basis up to $K_{\max} = 16$, and the source term contains the Fourier transform of the overlap between the ^{8}He and α-particle wave functions:

$$F_{^4\mathrm{n}}^{0^+} \sim \Phi_{^4\mathrm{n}}^{0^+} = \int \mathrm{d}\mathbf{r}\, e^{i\mathbf{qr}} \langle \Psi_\alpha | \Psi_{^8\mathrm{He}} \rangle \,, \tag{12}$$

where $\mathbf{r}$ is vector of the α-particle in the ^{8}He center-of-mass system. We consider here the COSMA model for the ^{8}He wave function and use only $K = K_{\min} = 2$ component in this source

$$\Phi_{^4\mathrm{n}}^{0^+}(\rho, \Omega_\rho) = \mathcal{J}_2(\Omega_\rho)\, \rho^2 \, \exp\left[-\rho^2/(2r_0^2)\right] \tag{13}$$

because we have found that only this component produces a noticeable response in the ^{4}n continuum. More details of the source term are given in appendix D.

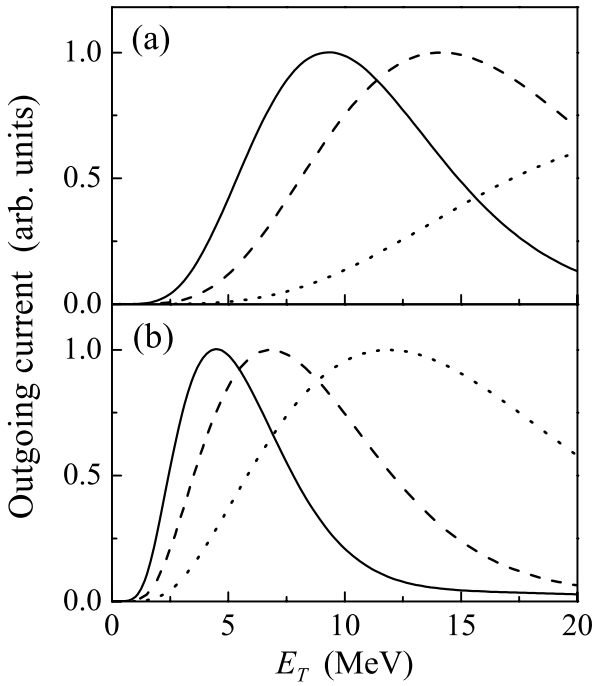

Fig. 11. Continuum response of the ^{4}n system in the MWS with a "Gaussian" source (13). Solid, dashed and dotted curves correspond to rms hyperradius $\langle\rho_{\rm sour}\rangle$ of the source equal to 8.9, 7.3, and 5.6 fm, respectively. Panels are calculated with (a) no final-state interaction, (b) RT potential (the correct n-n scattering length). All calculations are normalized to unity at the peak.

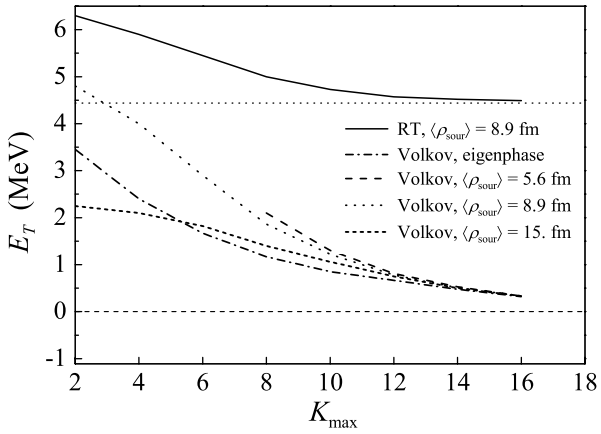

Fig. 12. Peak positions of the ^{4}n continuum response with RT (solid curve, $\langle\rho_{\rm sour}\rangle = 5.6$ fm), and Volkov V1 potentials (dashed curve $\langle\rho_{\rm sour}\rangle = 5.6$ fm, dotted curve $\langle\rho_{\rm sour}\rangle = 8.9$ fm, short-dashed curve $\langle\rho_{\rm sour}\rangle = 15$ fm). The horizontal dotted line is the convergence energy for the exponentially extrapolated solid curve. The lower limit of the plot corresponds to the threshold energy for $^4\mathrm{n} \to {}^2\mathrm{n} + {}^2$ n decay for Volkov potential.

In our calculations we used for the oscillator radius r_0 the value of 2.2 fm because this value gives the correct experimental radius of ^{8}He in the COSMA model. This value or r_0 corresponds to the rms hyperradius of the source

$$\langle\rho_{\rm sour}\rangle = \sqrt{n + 9/2}\; r_0$$

equal to 5.6 fm. Larger values of $\langle\rho_{\rm sour}\rangle$ were also used in this work to get a feeling of sensitivity to this parameter and to imitate a non-Gaussian tail of the source function.

Figure 11a shows the continuum responses which could be expected for sources of different sizes if no FSI was present in the ^{4}n system. This is a benchmark case [40] which is mainly determined by the internal structure of the source. To take FSI into account, we used the Reichstein and Tang potential (RT) [41] which provides the correct low-energy behaviour in the n-n channel. The interaction in odd partial waves was considered to be absent (the $u = 1$ case). It was shown in [33] that the net effect of this component of the n-n interaction is the weak repulsion which has very small effect on ^{4}n. The response functions obtained with $K_{\rm max} = 16$ have practically converged (see fig. 12). However, they strongly depend on the source size $\langle\rho_{\rm sour}\rangle$ (see fig. 11b). Comparing figs. 11a and b we can see that the four-neutron FSI has a pronounced effect on the continuum response. The FSI can shift the peak position to quite low energy. However, in order to shift it down to 4–5 MeV, a very large size of the source is required, which means that either the initial nucleus should be large, or the reaction mechanism should enhance the contribution from large distances, or both.

So, we see that the ^{4}n ground state cannot be interpreted as a real resonance, but still can be observed as some kind of a few-body continuum response in a reaction. This response should depend on the initial structure of the nuclei and the reaction mechanism, as well as on the ^{4}n FSI. Our calculations also give a clue as to why no signature of ^{4}n has been found in the pionic double charge exchange $^4\mathrm{He}(\pi^-, \pi^+)$. The source size in such a reaction should be comparable to the size of the α-particle, which would produce the ^{4}n missing-mass spectrum with maximum at energy around 30–40 MeV.

It could be of some methodological interest to see the results of calculations for ^{4}n with the Volkov V1 potential. This potential cannot be considered as realistic for calculations of the ^{4}n system as it makes the dineutron bound for about 0.55 MeV (which should lead to the overbinding of the whole system). Still it is often used in calculations of light nuclei and we can draw some qualitative conclusions for this example. The convergences of the peak positions of the energy distributions obtained in MWS with Volkov potential as functions of $K_{\rm max}$ included in the calculations, are shown by the dashed, dotted and short-dashed lines in fig. 12. Calculations were carried out with sources of different radii (even with unrealistic radius $\langle\rho_{\rm sour}\rangle = 15$ fm). We also made calculations of the $4 \to 4$ scattering searching for the energy behaviour of the eigenphases. The dot-dashed curve in fig. 12 shows the convergence of the energy, as a function of $K_{\rm max}$, where the lowest eigenphase is passing $\pi/2$.

As can be seen from fig. 12, for $K_{\rm max} < 14$ the calculated energies of the resonance depend strongly on

the particular model we consider. However, at $K_{\max} \geq 14$, where $E_{\rm T} < 0.5$ MeV, all calculations with the Volkov potential converge to each other and ^{4}n exists as an "ordinary" nuclear state. The actual energy of this state cannot be precisely determined in the present calculations because of the poor convergence of the HH method in the case of the V1 potential (for comparison, when the RT potential is used, the convergence of the HH method is much better, see the solid line in fig. 12). The reason for this is the presence of the two-body $^2\mathrm{n} + {}^2\mathrm{n}$ and three-body $^2\mathrm{n} + \mathrm{n} + \mathrm{n}$ channels in the ^{4}n system, the asymptotics of which are not treated explicitly in our HH calculations. The energy convergence of such HH calculations is known to be poor [15,16].

The rate at which the energy $E_{\rm T}$ decreases for the Volkov potential suggests that with the increase of $K_{\max}$ the converged energy may be either close to zero or have some negative value. However, we are pretty confident that this value should be above the $^2\mathrm{n} + {}^2\mathrm{n}$ threshold because quite a dramatic change of the Majorana part of the Volkov interaction is required to make ^{4}n bound with respect to the $^2\mathrm{n} + {}^2\mathrm{n}$ decay [32]. It is possible that, similar to the case of ^{5}H in the box of sect. 2.1, the ^{4}n state, obtained in our variational calculations without explicit treatment of cluster subsystems, will fall down to the lowest decay threshold $^2\mathrm{n} + {}^2\mathrm{n}$ in the limit of an infinite basis. Such a state would be located out of barriers and would have an unrealistically large radius. We have similar concerns with the use of Volkov forces (binding dineutron) for any system with two or more open neutron decay channels.

5 Conclusion

In this paper we have performed theoretical studies of broad states in few-body systems beyond the neutron drip line. We found that two different definitions of the width, i) as the width of the excitation spectrum and ii) as an inverse lifetime, diverge for broad states. In this sense the broad states do not possess important features which are typical for narrow states. However, they could be perfectly "observable" in reactions utilizing standard techniques as low-energy continuum responses.

We consider different procedures to define broad few-body ground-state properties and to find out at which continuum energy they converge (so that resonances can be considered as real ones). It occurs at about $E_{\rm T} = 0.5$ MeV both for ^{5}H and ^{4}n. Such energies are too low considering the realistic expectations for these nuclei. This fact is an indication that the observed properties of these nuclei can be strongly influenced by the observation conditions (reaction mechanism, etc.). So far, the theoretical studies implied that these systems can be treated as narrow states: they are described only by ground-state energy and (sometimes) width. Under the circumstances mentioned, this may be an oversimplification of the real situation.

To study properties of broad unbound states in the few-body systems we introduce the MWS model, which allows to incorporate such important ingredients as initial structure of colliding nuclei, reaction mechanism, few-body effects and final-state interactions. The MWS is used in this paper to explore qualitatively the sensitivity of the systems (^{5}H and ^{4}n) to different aspects of the model. It should be noted, however, that for high-energy reactions (the population of ^{5}H and ^{4}n by sudden removal of a nucleon or a cluster from the projectile) MWS becomes a good quantitative approximation.

We demonstrate that there are aspects of the dynamics for broad few-body states, which make them qualitatively different from broad two-body states. These aspects are slow motion in the internal region which is supplemented by multichannel and "shallow water" effects.

Studies of the sensitivity of the ^{5}H spectrum to reaction mechanism predict that the "ground state" peak may be observed at 2–3 MeV as lowest position, but may shift to much higher energies in certain situations. It is important that there exists a definite correlation (see figs. 3 and 4) between the shape of the energy spectrum of ^{5}H and the momentum correlations of ^{5}H decay products (measured, for example, in [5]).

In this work we provide the first large-basis continuum studies of the ^{4}n system. These studies give an explanation why no indication of ^{4}n FSI was found in the pion double charge exchange reactions and specify at which circumstances the sizable ^{4}n FSI effect should become observable.

We intend to discuss a situation with experimental studies of the ^{5}H system in the forthcoming paper [7], where also a more detailed account of the momentum correlations of the ^{5}H decay products will be given.

Numerous useful discussions with people involved in the experimental search for ^{5}H are acknowledged. We would like to mention here L. Chulkov, M. Golovkov, B. Jonson, A. Korsheninnikov, M. Meister, G. Nyman, Yu. Oganesuan, H. Simon and G. Ter-Akopian. The authors are thankful to B. Danilin, and N. Shulgina for discussions of theoretical aspects of the problem. The authors acknowledge the financial support from the Royal Swedish Academy of Science. The work was partly supported by the RFBR grants 00-15-96590 and 02-02-16174 and partially by the EPSRC grant GR/M/82141.

Appendix A. Notation of HH method

The details of the HH method and its application to a range of the light clusterized systems can be found in refs. [17,18,15,16,20,21]. The details of the models for ^{5}H and ^{4}n can be found in [8] and [9], respectively.

For ^{5}H the Jacobi vectors in "T" and in "Y" systems (see fig. 13) can be expressed in terms of the hyperradius ρ and the hyperangle θ_ρ:

$$\text{"T"}: \quad X = \sqrt{2}\,\rho \sin\theta_\rho, \qquad Y = \sqrt{5/6}\,\rho\cos\theta_\rho\,,$$

$$\text{"Y"}: \quad X = \sqrt{4/3}\,\rho \sin\theta_\rho, \qquad Y = \sqrt{5/4}\,\rho\cos\theta_\rho\,.$$

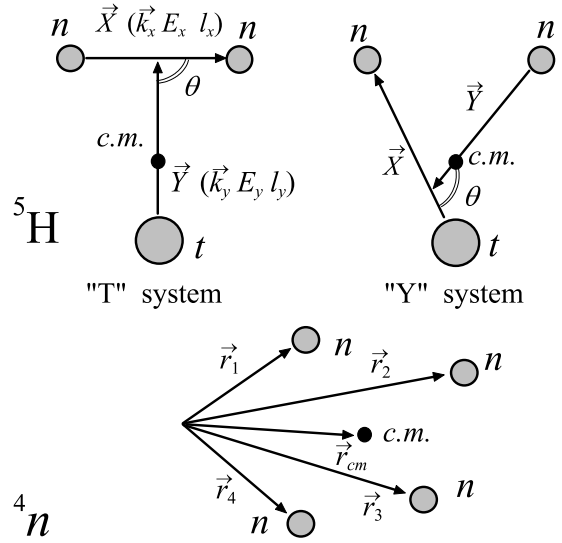

Fig. 13. Three-body model for ^{5}H and four-body model for ^{4}n. Coordinate systems as used in the article.

Analogically the Jacobi vectors in momentum space are defined via "momentum" κ and hyperangle θ_κ

$$E_{\rm T} = \kappa^2/2M, \quad E_x = E_{\rm T}\sin^2\theta_\kappa, \quad E_y = E_{\rm T}\cos^2\theta_\kappa\,,$$
$$\text{"T"}: \quad k_x = \sqrt{M/2\,E_x} \quad k_y = \sqrt{6M/5\,E_y}\,,$$
$$\text{"Y"}: \quad k_x = \sqrt{3M/4\,E_x} \quad k_y = \sqrt{4M/5\,E_y}\,,$$

where M is a "scaling" nucleon mass. Hyperangles θ_ρ and θ_κ should be distinguished from the angle θ between Jacobi vectors $\mathbf{X}$ and $\mathbf{Y}$ in the real coordinate space.

The wave function (WF) of the $3 \to 3$ scattering can be written as

$$\Psi_3^{JM} = \sqrt{\frac{2}{\pi}}\frac{(2\pi)^3}{(\kappa\rho)^{5/2}}\sum_{K\gamma} i^K \Big\{ \sum_{K'\gamma'} \chi_{K\gamma}^{K'\gamma'}(\kappa\rho)\mathcal{J}_{K'\gamma'}^{JM}(\Omega_\rho)\Big\} \times \textstyle\sum_{M_L M_S M_{S_x} m_3} C^{JM}_{LM_L SM_S}\,\mathcal{I}^{LM_L}_{Kl_x l_y}(\Omega_\kappa)\,,$$

where K is the generalized angular-momentum quantum number, and the following shortcuts are used:

$$\gamma = \{L, l_x, l_y, S, S_x\}\,,$$
$$\Omega_\rho = \{\theta_\rho, \hat{X}, \hat{Y}\}\,, \quad \Omega_\kappa = \{\theta_\kappa, \hat{k}_x, \hat{k}_y\}\,.$$

The hyperspherical functions depending on 5 angles and spin variables are defined as

$$\mathcal{J}^{JM}_{KLSS_x l_x l_y}(\Omega_\rho) = \left[\mathcal{I}^{LM_L}_{Kl_x l_y}(\Omega_\rho)\otimes X_{SS_x}\right]_{JM}\,,$$

where X_{SS_x} is the coupled spin function of two neutrons S_x and a core $S_3 = 1/2$,

$$X_{SS_x M_S} = \left[\left[\chi_{S_1}\otimes\chi_{S_2}\right]_{S_x}\otimes\chi_{S_3}\right]_{SM_s}\,,$$

where χ_{S_i} includes spins of nucleons or constituent clusters and

$$\mathcal{I}^{LM_L}_{Kl_x l_y}(\Omega_\rho) = \psi_K^{l_x l_y}(\theta_\rho)\left[Y_{l_x}(\hat{x})\otimes Y_{l_y}(\hat{y})\right]_{LM_L}\,.$$

The hyperangular eigenfunctions $\psi_K^{l_x l_y}$ are proportional to the Jacobi polynomials $P_n^{\alpha,\beta}$,

$$\psi_K^{l_x l_y}(\theta_i) = N_K^{l_x l_y}(\sin\theta_i)^{l_x}(\cos\theta_i)^{l_y}P^{l_x+1/2,l_y+1/2}_{(K-l_x-l_y)/2}(\cos 2\theta_i)\,. \tag{A.1}$$

The asymptotic behaviour of the functions $\chi(\kappa\rho)$ at large ρ values is

$$\chi_{K\gamma}^{K'\gamma'}(\kappa\rho) \sim \delta_{K\gamma}^{K'\gamma'}\,\mathcal{H}^{(-)}_{K+3/2}(\kappa\rho) - S_{K\gamma}^{K'\gamma'}\,\mathcal{H}^{(+)}_{K+3/2}(\kappa\rho)\,.$$

Here $\mathcal{H}^{(\mp)}_{K+3/2}$ are the Riccati-Bessel functions of half-integer index, with asymptotic $\sim \exp[\mp i\kappa\rho]$, describing the in and outgoing three-body spherical waves. $S_{K\gamma}^{K'\gamma'}$ is the S-matrix for the $3 \to 3$ scattering.

A WF with pure outgoing asymptotic and real energy can be obtained only as a solution of the inhomogeneous equation. For three particles it has the form

$$\Psi_3^{JM(+)} = \rho^{-5/2}\textstyle\sum_{K\gamma}\,\chi^{(+)}_{K\gamma}(\kappa\rho)\,\mathcal{J}^{JM}_{K\gamma}(\Omega_\rho)\,\mathcal{J}^{JM}_{K\gamma}(\Omega_\kappa)\,. \tag{A.2}$$

The radial components of this WF at large ρ values behave as

$$\chi^{(+)}_{K\gamma}(\kappa\rho) \sim A^{KSS_x}_{Ll_x l_y}(\kappa)\,\mathcal{H}^{(+)}_{K+3/2}(\kappa\rho)\,, \tag{A.3}$$

where the asymptotic amplitudes $A^{KSS_x}_{Ll_x l_y}$ are defined by the nature of the source.

For four identical particles the hyperradius is defined via single-particle coordinates as

$$\textstyle\sum_{i=1,4} r_i^2 = \rho^2 + 4r_{\rm cm}^2\,. \tag{A.4}$$

A WF with outgoing asymptotic has the form

$$\Psi_4^{JM(+)} = \rho^{-4}\textstyle\sum_{K\gamma}\,\chi^{(+)}_{K\gamma}(\kappa\rho)\,\mathcal{J}^{JM}_{K\gamma}(\Omega_\rho)\,\mathcal{J}^{JM}_{K\gamma}(\Omega_\kappa)\,,$$

where at large ρ values $\chi^{(+)}_{K\gamma}(\kappa\rho) \sim A^K_\gamma\,\mathcal{H}^+_{K+3}(\kappa\rho)$. For four identical particles the hyperspherical harmonics $\mathcal{J}^{JM}_{K\gamma}$ are antisymmetrized [9]; for simplicity, we do not specify their index γ here.

On the hyperspherical basis the variational procedure reduces the Schrödinger equation with the inhomogeneous term $\left(\hat{H}_A - E_{\rm T}\right) = F$ for A particles to a set of coupled ordinary differential equations:

$$\left[\frac{{\rm d}^2}{{\rm d}\rho^2} - \frac{\mathcal{L}(\mathcal{L}+1)}{\rho^2} + 2M\left\{E_{\rm T} - V_{K\gamma,K\gamma}(\rho)\right\}\right]\chi_{K\gamma}(\rho) = \sum_{K'\gamma'} 2MV_{K\gamma,K'\gamma'}(\rho)\chi_{K'\gamma'}(\rho) + f_{K\gamma}(\rho)\,, \tag{A.5}$$

$$V_{K\gamma,K'\gamma'}(\rho) = \int {\rm d}\Omega_\rho\;\mathcal{J}^\dagger_{K\gamma}(\Omega_\rho)\left[\sum_{i>j}\hat{V}(\mathbf{r}_{ij})\right]\mathcal{J}_{K'\gamma'}(\Omega_\rho)\,,$$

where $\mathcal{L} = K + (3A-6)/2$. The functions $f_{K\gamma}(\rho)$ are terms of the hyperspherical expansion of the inhomogeneous term F:

$$f_{K\gamma}(\rho) = \rho^{(3A-4)/2}\int {\rm d}\Omega_\rho\,\mathcal{J}^\dagger_{K\gamma}(\Omega_\rho)\,F(\rho,\Omega_\rho)\,.$$

Appendix B. Approximations required to obtain MWS in the general case

It is methodologically important to find valid approximations to reduce a realistic reaction model to MWS. Below we discuss these approximations and obtain expressions for cross-sections via MWS WFs.

In the nuclear reaction $A + B \to F + R$ a few-body continuum F (channel function Ψ_{FR}; let it be a three-body continuum for clarity) is populated in a two-body reaction (channel function Ψ_{AB}) and identified by means of a recoil particle R (missing-mass experiment). The total WF can be written as

$$\Psi = \Psi_{AB} + \Psi_{FR}^{(+)} .$$

The superscript (+) in the function $\Psi_{FR}^{(+)}$ emphasises the fact that in this channel there are only functions with outgoing asymptotic. The asymptotic form of the WFs Ψ_{AB} and $\Psi_{FR}^{(+)}$ is explicitly clusterized:

$$\Psi_{AB} = \psi_A \psi_B \psi_{AB}, \qquad \Psi_{FR} = \psi_{FR}^{(+)} \psi_R ,$$

where ψ_A, ψ_B, ψ_R are the internal WFs of the target, projectile and recoil fragment. The function $\psi_{FR}^{(+)}$ combines the WF of the few-body subsystem of interest and WF of relative motion with recoil nucleus. Use of such factorised WFs in the whole space is the first approximation we make here. The system of coupled equations in the subspaces AB and FR then reads

$$\begin{cases} \left(\hat{H}_{AB} - E_{AB}\right) \psi_{AB} = \langle \psi_A \psi_B | \hat{V} | \Psi_{FR} \rangle, \\ \left(\hat{H}_{FR} - E_{FR}\right) \psi_{FR}^{(+)} = \langle \psi_R | \hat{V} | \Psi_{AB} \rangle. \end{cases}$$

Here the cluster energies are already subtracted and E_{AB}, E_{FR} are the energies relative to the corresponding cluster break-up threshold. The energy E_{FR} in the break-up channel is directly related to the energy in the incoming channel $E_{FR} = E_{AB} - Q$, where Q is the threshold difference. The operator $\hat{V}$ is the sum of all the pairwise nucleon-nucleon interactions in the system. The above system of equations is reduced to the subspace FR if the few-body break-up channel is only a perturbation for the two-body incoming channel ($\|\Psi_{AB}\| \gg \|\Psi_{FR}^{(+)}\|$ in the internal region)

$$\left(\hat{H}_{FR} - E_{FR}\right) \psi_{FR}^{(+)}(\overline{\rho}, \mathbf{r}) = F(\overline{\rho}, \mathbf{r}) , \qquad \text{(B.1)}$$

where the notation $F(\overline{\rho}, \mathbf{r})$ is used for overlap integral $\langle \psi_R | \hat{V} | \Psi_{AB} \rangle$ and $\overline{\rho} = \{\rho, \Omega_\rho\}$ is a set of 6 variables of the three-body subsystem.

We now split the WF $\psi_{FR}^{(+)}(\overline{\rho}, \mathbf{r})$ into two parts:

$$\psi_{FR}^{(+)}(\overline{\rho}, \mathbf{r}) = \psi_0^{(+)}(\overline{\rho}, \mathbf{r}) + \psi_1^{(+)}(\overline{\rho}, \mathbf{r})$$

the first of which is found in the approximation which is close in the spirit to the Migdal-Watson model. For that purpose we use the auxiliary Hamiltonian $\hat{H}'_{FR}$

$$\hat{H}_{FR} = \hat{H}'_{FR} + \Delta\hat{V} ,$$

where $\Delta\hat{V}$ includes all the interactions between the recoil nucleus and the few-body system. We look for $\psi_0^{(+)}$ as solution with reduced Hamiltonian $\hat{H}'_{FR}$. As far as the subsystems F and R are not interacting in $\hat{H}'_{FR}$, the WF $\psi_0^{(+)}$ can be written as

$$\psi_0^{(+)}(\overline{\rho}, \mathbf{r}) = (2\pi i)^{-1} \int\limits_{-\infty}^{\infty} \mathrm{d}\varepsilon \int \mathrm{d}\overline{\rho}' \, \mathrm{d}\mathbf{r}' \, G_\varepsilon^{(+)}(\overline{\rho}, \overline{\rho}') \times G_{E_{FR}-\varepsilon}^{(+)}(\mathbf{r}, \mathbf{r}') \, F(\overline{\rho}', \mathbf{r}') .$$

First, the two-body Green's function acts on the source. For radii r larger than the source size this operation gives

$$\psi_0^{(+)}(\overline{\rho}, \mathbf{r}) = \frac{m}{\pi i} \int\limits_{-\infty}^{\infty} \mathrm{d}\varepsilon \, \frac{\chi_{k(\varepsilon)l}^{(+)}(r)}{r} \, Y_{lm}(\hat{r}) \times \int \mathrm{d}\overline{\rho}' \, G_\varepsilon^{(+)}(\overline{\rho}, \overline{\rho}') \, F_{lm}(\overline{\rho}', k(\varepsilon)),$$

where $k(\varepsilon) = \sqrt{2m(E_{FR} - \varepsilon)}$ and the three-body source is

$$F_{lm}(\overline{\rho}, k(\varepsilon)) = \int \frac{\chi_{kl}(r)}{rk} Y_{lm}^*(\hat{r}) F(\overline{\rho}, \mathbf{r}) \, \mathrm{d}\mathbf{r}. \qquad \text{(B.2)}$$

In the second stage the source and the three-body Green's function $G_\varepsilon^{(+)}(\overline{\rho}, \overline{\rho}')$ are replaced by the solution of the inhomogeneous three-body equation,

$$\psi_0^{(+)}(\overline{\rho}, \mathbf{r}) = \frac{m}{\pi i} \int\limits_{-\infty}^{\infty} \mathrm{d}\varepsilon \, \Psi_{\varepsilon lm}^{JM(+)}(\overline{\rho}\,) \frac{\chi_{k(\varepsilon)l}^{(+)}(r)}{r} Y_{lm}(\hat{r}) .$$

Here WF $\Psi_{\varepsilon lm}^{JM(+)}(\overline{\rho})$ is the solution of the equation

$$(\hat{H}_3 - \varepsilon) \Psi_{\varepsilon lm}^{JM(+)}(\overline{\rho}\,) = F_{lm}(\overline{\rho}, k(\varepsilon)) ,$$

which is defined in (A.2). The hyperspherical components of this solution are marked not only by the quantum numbers $K\gamma$ of the three-body problem, but also by the quantum numbers lm of the recoil channel. It should be noted that in the general case the function F can be very complicated. It contains the information about the reaction mechanism, the total available energy, the angular momentum and the energy distribution in the recoil channel.

The break-up cross-section is defined by a particle's flux $j_R(a)$ through a sphere of a large radius a. This can be defined using any particle. For example, for the recoil nucleus R

$$j_R(a) = \frac{1}{m} \mathrm{Im} \int r^2 \mathrm{d}\Omega_r \mathrm{d}\overline{\rho} \, \psi_0^{(+)\dagger}(\overline{\rho}, \mathbf{r}) \nabla_r \psi_0^{(+)}(\overline{\rho}, \mathbf{r}) \Big|_{r=a} .$$

Using the definition (A.2) and the asymptotic normalization condition (A.3) we obtain

$$j_R(a) = \frac{m^2}{2\pi} \int\limits_0^{E_{FR}} \mathrm{d}\varepsilon \frac{k(\varepsilon)}{m} \frac{\kappa(\varepsilon)}{M} \sum_{K\gamma lm} |A_{K\gamma lm}(\varepsilon)|^2 ,$$

where $\kappa(\varepsilon) = \sqrt{2M\varepsilon}$. The energy integration limits are now ranging from 0 to E_{FR} as WFs with energies outside

of this interval do not contribute to the outgoing wave. The distribution of the energy between few-body subsystem and the recoil particle in the WF $\psi_0^{(+)}(\overline{\rho},\mathbf{r})$ is thus given by

$$\frac{\mathrm{d}j}{\mathrm{d}\varepsilon} = \frac{1}{\pi}\frac{m^{3/2}}{M^{1/2}}\sqrt{\varepsilon(E_{FR}-\varepsilon)}\sum_{K\gamma lm}|A_{K\gamma lm}(\varepsilon)|^2 \ .$$

This expression gives the connection between values calculated in MWS (amplitudes $A_{K\gamma lm}(\varepsilon)$) and observables for a reaction with definite kinematical conditions.

The next step is to find the corrections to the function $\psi_0^{(+)}(\rho,\mathbf{r})$ taking into account the full dynamics of the system. The function $\psi_1^{(+)}(\rho,\mathbf{r})$ is given by

$$\left(\hat{H}_{FR}-E_{FR}\right)\psi_1^{(+)}(\overline{\rho},\mathbf{r}) = \Delta\hat{V}\psi_0^{(+)}(\overline{\rho},\mathbf{r})\,.$$

The condition under which this correction is small is the kinematic separation of the subsystems: the typical energy in the few-body subsystem should be much less than in the recoil channel. Then the function $\psi_0^{(+)}(\rho,\mathbf{r})$ is strongly oscillating with respect to the variable r and the source for the function $\psi_1^{(+)}$ becomes effectively weak. This is normally assumed in the Migdal-Watson approximation. The sudden-removal approximation discussed in the following appendices implies large momentum transfer to the recoil and is a limiting case of the approximation given here.

Another situation in which the addition of the function $\psi_1^{(+)}(\rho,\mathbf{r})$ would not change qualitatively the observables is when the states in the few-body subsystem are very narrow compared to the energetically allowed region. However, in this paper we are interested in the opposite situation.

Appendix C. Sudden removal of a proton from ^{6}He

To substantiate the MWS model, we are going to obtain an expression for the source function in the approximation of the sudden removal of a proton from ^{6}He. We consider the ^{6}He WF in the COSMA model approximation [17] which makes the analytical treatment of the problem possible. Only $K=0$ and $K=2$ components with $S=0$ are taken into account,

$$\Psi_{^6\mathrm{He}}(\mathbf{X},\mathbf{Y}) = \frac{4}{\sqrt{\pi}r_{\mathrm{He}}^3}\left(A_0+\frac{2A_2}{\sqrt{3}r_{\mathrm{He}}^2}\left(Y^2-X^2/4\right)\right)$$
$$\times\exp\left[-(Y^2+X^2/4)/r_{\mathrm{He}}^2\right](4\pi)^{-1}\chi_{S=0}^{nn}\Psi_\alpha \ , \qquad \text{(C.1)}$$

where χ_S^{nn} is spin function of the valence neutrons and A_K is the amplitude of the component with hyperspherical moment K. The three-body calculations show that both amplitudes are positive and the weights of components are about $A_0^2\approx 0.05$ and $A_2^2\approx 0.77$. The rms matter radius of ^{6}He is reproduced with experimental rms matter radius of the α-particle $r_{\mathrm{mat}}(\alpha)=1.46$ and the oscillator

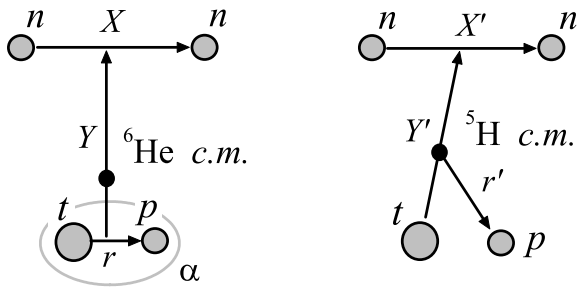

Fig. 14. Jacobi coordinate sets for the description of the removal of a proton from ^{6}He to form ^{5}H.

parameter of the valence nucleons $r_{\mathrm{He}}=2.73$ fm [17]. The WF is normalized for integration over $\mathrm{d}^3X\mathrm{d}^3Y$. The ^{6}He WF approximated in this way mimics well the geometry of the realistic three-body WF and is a reasonable approximation for observables which are not very sensitive to the asymptotic properties of the WF. We assume that the proton motion in the α-particle can be described by an oscillator WF as well:

$$\Psi_\alpha(\mathbf{r}) = \frac{2}{\pi^{1/4}r_\alpha^{3/2}}\exp\left[-\frac{r^2}{2r_\alpha^2}\right]\frac{1}{\sqrt{4\pi}}\chi_{S=0}^{tp}\Psi_t \ . \qquad \text{(C.2)}$$

The WF is normalized for integration over d^3r. Here Ψ_t is internal triton WF, χ_S^{tp} is a spin function of a proton and a triton and the oscillator parameter

$$r_\alpha = (4/3)\sqrt{2/3}\,r_{\mathrm{mat}}(\alpha) = 1.59\,\mathrm{fm}$$

should be chosen to provide the experimental rms radius for the proton in the α-particle.

To study the sudden removal of the proton we should transfer the WF (C.1), (C.2) to a coordinate system, where the proton motion is considered from the total center of mass (fig. 14):

$$\mathbf{X}=\mathbf{X}' \ , \quad \mathbf{Y}=\frac{9}{10}\mathbf{Y}'-\frac{1}{4}\mathbf{r}' \ , \quad \mathbf{r}=\frac{2}{5}\mathbf{Y}'+\mathbf{r}' \ . \qquad \text{(C.3)}$$

The new set of Jacobi coordinates $\mathbf{X}'$ and $\mathbf{Y}'$ corresponds to the internal motion of ^{5}H. The momentum distribution of ^{5}H center of mass is given by the Fourier transform of the WF (C.1) over the coordinate $\mathbf{r}'$. A projection of this transform on the zero angular momentum in coordinate r' allows to find spatial configurations which populate the ground state of ^{5}H:

$$\Phi_{^5\mathrm{H}}^{1/2^+}(\mathbf{X}',\mathbf{Y}',\mathbf{q})$$
$$= \int \mathrm{d}\Omega_q Y_{00}(\hat{q})\int \mathrm{d}^3r' e^{i\mathbf{q}\mathbf{r}'}\langle\Psi_t|\Psi_{^6\mathrm{He}}(\mathbf{X}',\mathbf{Y}',\mathbf{r}')\rangle$$
$$= (4\pi)^{-1}\chi_{S=1/2}^{tnn}\Psi_t\left[(A_0F_1(qY')+A_2F_2(qY'))\right.$$
$$\left.+\frac{2A_2}{\sqrt{3}r_{\mathrm{He}}^2}\left(\tfrac{64x^4}{(1+8x^2)^2}Y'^2-\tfrac{1}{4}X'^2\right)F_1(qY')\right]F(q)$$
$$\times\exp\left[-(\tfrac{8x^2}{1+8x^2}Y'^2+\tfrac{1}{4}X'^2)/r_{\mathrm{He}}^2\right] \ , \qquad \text{(C.4)}$$

where $x = r_{\rm He}/r_\alpha$ and should be around 1.7 for a realistic geometry of the α-particle. $\chi^{tnn}_{S=1/2}$ is a total spin function with two neutron coupled to $S = 0$. Functions F_0 and F_1 tend to constants at low qY' values and

$$F(q) = \frac{4\pi}{\sqrt{\pi^{3/2} r_\alpha^3}} \frac{64}{(1+8x^2)^{3/2}} \exp\left[-\frac{4r_{\rm He}^2 q^2}{1+8x^2}\right]. \quad \text{(C.5)}$$

In the limit of low momentum q transferred to ^{5}H center of mass (practical requirement is $q < 50$ MeV/c) this expression has a factorised form

$$\Phi^{1/2^+}_{^5{\rm H}}(\mathbf{X}', \mathbf{Y}', \mathbf{q}) = \Phi^{1/2^+}_{^5{\rm H}}(\mathbf{X}', \mathbf{Y}') F(q), \quad \text{(C.6)}$$

where

$$\Phi^{1/2^+}_{^5{\rm H}}(\mathbf{X}', \mathbf{Y}') = (4\pi)^{-1} \times \chi^{tnn}_{S=1/2} \Psi_t \exp\left[-\left(\tfrac{8x^2}{8x^2+1} Y'^2 + \tfrac{1}{4} X'^2\right)/r_{\rm He}^2\right] \times \left[\left(A_0 + A_2 \tfrac{\sqrt{3}}{1+8x^2}\right) + \frac{2A_2}{\sqrt{3} r_{\rm He}^2}\left(\tfrac{64x^4}{(8x^2+1)^2} Y'^2 - \tfrac{1}{4} X'^2\right)\right]. \quad \text{(C.7)}$$

A transformation of such spatial configuration using the eigenfunctions of the ^{5}H Hamiltonian with $J^\pi = 1/2^+$ will give momentum distributions of particles in the ^{5}H continuum corresponding to its ground state. Technically we realize this by solving the inhomogeneous equation (4). It should be noted that the theoretical technique, which we use in this paper, is a generalization of the technique used in papers [42,43].

The components of the source function, eq. (C.7), have a very high similarity with the components of ^{6}He WF, eq. (C.1), in the sense of their geometry. However, the relative contributions of these components can be significantly affected by the reaction mechanism. Even in the simple reaction mechanism assumed ($q \to 0$), the relative weight of the $K = 0$ component in the source function can be 1.5–2 times larger than in the initial WF. We can see that the assumption of eq. (5), which seem to be oversimplified, in reality can be quantitatively connected with a realistic scenario of the ^{5}H population.

Appendix D. Sudden removal of the α-particle from ^{8}He

In this section we are deducing the possible properties of the source function for ^{4}n in the example of sudden removal of the core from the four-neutron halo nucleus (here ^{8}He). The ^{8}He WF is considered in the COSMA approximation [39] as ^{6}He WF in the previous section:

$$\Psi_{^8{\rm He}} = \frac{1}{\sqrt{4!}} \det\left(\prod_{i=1,4} \Psi_{m_j}(\mathbf{r}_i)\right) \Psi_\alpha, \quad \text{(D.1)}$$

where Ψ_α is the internal WF of the α-particle, Ψ_j are single-nucleon WFs depending on coordinates $\mathbf{r}_i$ from the α-particle having total $j = 3/2$ and different m_j projections:

$$\Psi_{m_j}(\mathbf{r}_i) = \sqrt{\frac{8}{3\sqrt{\pi} r_{\rm He}^5}}\, r_i \exp\left[-\frac{r_i^2}{2r_{\rm He}^2}\right] \left[Y_1(\hat{r}_i) \otimes \chi_{1/2}\right]_{jm_j}. \quad \text{(D.2)}$$

The parameter $r_{\rm He}$, which reproduces the rms matter radius of ^{8}He is 2.2 fm. The nucleon rms radius for this WF is $\langle r \rangle = \sqrt{5/2}\, r_{\rm He} = 3.48$ fm.

The above WF can be rewritten in the variables ρ (hyperradius of ^{4}n), Ω (angles and hyperangles of ^{4}n), and $\mathbf{r}'$ (relative motion of ^{4}n and α-particle). These variables are defined by eq. (A.4) and the transformation of the volume element from single-particle coordinates, fig. 13, to the ^{4}n center-of-mass coordinates and the hyperspherical coordinates is

$$\mathrm{d}^3 r_2 \mathrm{d}^3 r_2 \mathrm{d}^3 r_3 \mathrm{d}^3 r_4 = 2\, \mathrm{d}^3 r_{\rm cm}\, \rho^8 \mathrm{d}\rho\, \mathrm{d}\Omega_\rho.$$

The momentum distribution of the ^{4}n 0^+ cm motion in the sudden-removal approximation is obtained as the Fourier transform of the WF (D.1) over the coordinate r' of the α-^{4}n motion and projecting that to zero angular momentum. The obtained source function is

$$\Phi^{0^+}_{^4{\rm n}}(\rho, \Omega, \mathbf{q}) = \int \mathrm{d}\Omega_q Y_{00}(\hat{q}) \int \mathrm{d}^3 r' e^{i\mathbf{q}\mathbf{r}'} \langle \Psi_\alpha | \Psi_{^8{\rm He}}(\rho, \Omega, \mathbf{r}') \rangle = \left(A_2 \rho^2 \mathcal{J}_2(\Omega) F_2(q) + A_4 \rho^4 \mathcal{J}_4(\Omega) F_4(q)\right) \exp\left[-\frac{\rho^2}{2r_{\rm He}^2}\right],$$

where $\mathcal{J}_2$ is the four-neutron antisymmetrized hyperspherical harmonic with $K = 2$, $\mathcal{J}_4$ is some linear combination of two possible $K = 4$ HHs, and the formfactors are

$$F_2(q) = \left(\frac{\pi}{2}\right)^{3/2} \frac{4}{9\pi r_{\rm He}^5} (12 - q^2 r_{\rm He}^2) \exp\left[-q^2 r_{\rm He}^2/8\right],$$

$$F_4(q) = \left(\frac{\pi}{2}\right)^{3/2} \frac{64}{9\pi r_{\rm He}^7} \exp\left[-q^2 r_{\rm He}^2/8\right].$$

Calculations show that only the $K = 2$ component of the source function significantly populate the ^{4}n continuum. For that reason the ratio of the coefficients A_2 and A_4 is not important for us.

References

1. B. Jonson *et al.*, Phys. Rep. **389**, 1 (2004).
2. A.A. Korsheninnikov *et al.*, Phys. Lett. B **326**, 31 (1994).
3. A.A. Korsheninnikov *et al.*, Phys. Rev. Lett. **87**, 092501 (2001).
4. M. Golovkov *et al.*, Phys. Lett. B **566**, 70 (2003).
5. M. Meister *et al.*, Nucl. Phys. A **723**, 13 (2003); Phys. Rev. Lett. **91**, 162504 (2003).
6. A.A. Korsheninnikov *et al.*, Phys. Rev. Lett. **90**, 082501 (2003).
7. L.V. Grigorenko, to be published in Eur. Phys. J. A.
8. N.B. Shul'gina, B.V. Danilin, L.V. Grigorenko, M.V. Zhukov, J.M. Bang, Phys. Rev. C **62**, 014312 (2000).
9. N.K. Timofeyuk, Phys. Rev. C **65**, 064306 (2002).

10. J.J. Bevelacqua, Nucl. Phys. A **357**, 126 (1981).
11. N.A.F.M. Poppelier, L.D. Wood, P.W.M. Glaudemans, Phys. Lett. B **157**, 120 (1985).
12. A.M. Gorbatov *et al.*, Yad. Fiz. **50**, 347 (1989) (Sov. J. Nucl. Phys. **50**, 218 (1989)).
13. G.F. Filippov, A.D. Bazavov, K. Kato, Yad. Fiz. **62**, 1763 (1999) (Phys. At. Nucl. **62**, 1642 (1999)).
14. P. Descouvemont, A. Kharbach, Phys. Rev. C **63**, 027001 (2001).
15. L.V. Grigorenko, B.V. Danilin, V.D. Efros, N.B. Shul'gina, M.V. Zhukov, Phys. Rev. C **57**, R2099 (1998).
16. L.V. Grigorenko, B.V. Danilin, V.D. Efros, N.B. Shul'gina, M.V. Zhukov, Phys. Rev. C **60**, 044312 (1999).
17. M.V. Zhukov, B.V. Danilin, D.V. Fedorov, J.M. Bang, I.J. Thompson, J.S. Vaagen, Phys. Rep. **231**, 151 (1993).
18. B.V. Danilin, I.J. Thompson, J.S. Vaagen, M.V. Zhukov, Nucl. Phys. A **632**, 383 (1998).
19. D.H. Boal, C. Gelbke, B.K. Jennings, Rev. Mod. Phys. **62**, 553 (1990).
20. L.V. Grigorenko, R.C. Johnson, I.G. Mukha, I.J. Thompson, M.V. Zhukov, Phys. Rev. Lett. **85**, 22 (2000).
21. L.V. Grigorenko, R.C. Johnson, I.G. Mukha, I.J. Thompson, M.V. Zhukov, Phys. Rev. C **64**, 054002 (2001).
22. A.I. Baz, Zh. Eksp. Teor. Fiz. **70**, 397 (1976).
23. S. Flügge, *Practical Quantum Mechanics* (Springer, Berlin, 1971).
24. J.E. Ungar *et al.*, Phys. Lett. B **144**, 333 (1984).
25. T.P. Gorringe *et al.*, Phys. Rev. C **40**, 2390 (1989).
26. A.V. Belozyorov *et al.*, Nucl. Phys. A **477**, 131 (1988).
27. D.V. Aleksandrov *et al.*, Yad. Fiz. **47**, 3 (1988).
28. F. M. Marqués *et al.*, Phys. Rev. C **65**, 044006 (2002).
29. J.J. Bevelacqua, Nucl. Phys. A **341**, 414 (1980).
30. R.Ya. Kezerashvili, Yad. Fiz. **44**, 842 (1986) (Sov. J. Nucl. Phys. **44**, 542 (1986)).
31. A.M. Gorbatov *et al.*, Yad. Fiz. **50**, 962 (1989) (Sov. J. Nucl. Phys. **50**, 1551 (1989)).
32. N.K. Timofeyuk, J. Phys. G **29**, L9 (2003).
33. S.C. Pieper, Phys. Rev. Lett. **90**, 252501 (2003).
34. R.I. Jibuti, R.Ya. Kezerashvili, K.I. Sigua, Yad. Fiz. **32**, 1536 (1980).
35. R.I. Jibuti, R.Ya. Kezerashvili, K.I. Sigua, Phys. Lett. B **102**, 381 (1981).
36. A.M. Badalyan, T.I. Belova, N.B. Konyuhova, V.D. Efros, Yad. Fiz. **41**, 1460 (1985) (Sov. J. Nucl. Phys. **41**, 926 (1985)).
37. I.F. Gutich, A.V. Nesterov, I.P. Okhrimenko, Yad. Fiz. **50**, 19 (1989).
38. S.A. Sofianos, S.A. Rakityansky, G.P. Vermaak, J. Phys. G **23**, 1619 (1997).
39. M.V. Zhukov, A.A. Korsheninnikov, M.H. Smedberg, Phys. Rev. C **50**, R1 (1994).
40. C. Forssen, B. Jonson, M.V. Zhukov, Nucl. Phys. A **673**, 143 (2000).
41. I. Reichstein, Y.C. Tang, Nucl. Phys. A **139**, 144 (1969).
42. M. Zinser *et al.*, Phys. Rev. Lett. **75**, 1719 (1995).
43. M. Thoennessen *et al.*, Phys. Rev. C **59**, 111 (1999).